1.9 The net current flowing at the equilibrium potential is zero, yet this is a dynamic situation with equal opposing cathodic and anodic current components (whose absolute value is i_0). Suggest an experimental route for estimating the value of i_0.

1.10 Explain clearly why only a fraction of the energy shift (associated with a potential shift) is used for increasing the activation energy barrier.

REFERENCES

1. Maloy, J. R., *J. Chem. Educ.* **60**, 285 (1983).
2. Smith, M. G., *Laplace Transform Theory*, Van Nostrand, London, 1966.
3. Compton, R. G.; Eklund, J.; Marken, F., *Electroanalysis* **9**, 509 (1997).
4. Grundler, P.; Kirbs, A., *Electroanalysis* **11**, 223 (1999).
5. Grahame, D., *Chem. Rev.* **41**, 441 (1947).
6. Swietlow, A.; Skoog, M.; Johansson, G., *Electroanalysis* **4**, 921 (1992).
7. Grahame, D. C., *Ann. Rev. Phys. Chem.* **6**, 337 (1955).
8. Mohilner, D., *J. Electroanal. Chem.* **1**, 241 (1966).
9. Bockris, O'M.; Devanathan, M. A.; Muller, K., *Proc. Roy. Soc. Lond.* **55**, A274 (1963).
10. Parsons, R., *J. Electrochem. Soc.* **127**, 176C (1980).
11. Mark, H. B., *Analyst* **115**, 667 (1990).
12. Bond, A. M.; Heritage, I.; Briggs, M., *Langmuir* **1**, 110 (1985).

2

STUDY OF ELECTRODE REACTIONS AND INTERFACIAL PROPERTIES

2.1 CYCLIC VOLTAMMETRY

Cyclic voltammetry is the most widely used technique for acquiring qualitative information about electrochemical reactions. The power of cyclic voltammetry results from its ability to rapidly provide considerable information on the thermodynamics of redox processes and the kinetics of heterogeneous electron transfer reactions and on coupled chemical reactions or adsorption processes. Cyclic voltammetry is often the first experiment performed in an electroanalytical study. In particular, it offers a rapid location of redox potentials of the electroactive species, and convenient evaluation of the effect of media on the redox process.

Cyclic voltammetry consists of scanning linearly the potential of a stationary working electrode (in an unstirred solution), using a triangular potential waveform (Fig. 2.1). Depending on the information sought, single or multiple cycles can be used. During the potential sweep, the potentiostat measures the current resulting from the applied potential. The resulting current–potential plot is termed a *cyclic voltammogram*. The cyclic voltammogram is a complicated, time-dependent function of a large number of physical and chemical parameters.

Figure 2.2 illustrates the expected response of a reversible redox couple during a single potential cycle. It is assumed that only the oxidized form O is present initially. Thus, a negative-going potential scan is chosen for the first half-cycle, starting from a value where no reduction occurs. As the applied

Analytical Electrochemistry, Third Edition, by Joseph Wang

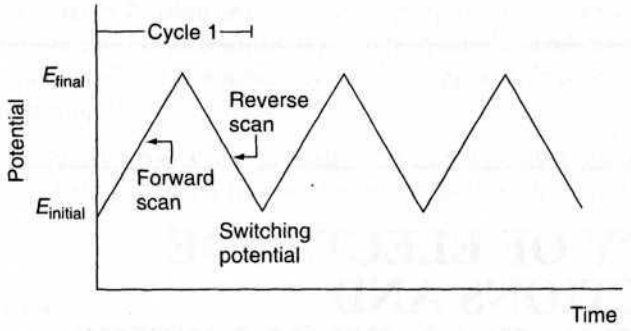

Figure 2.1 Potential–time excitation signal in a cyclic voltammetric experiment.

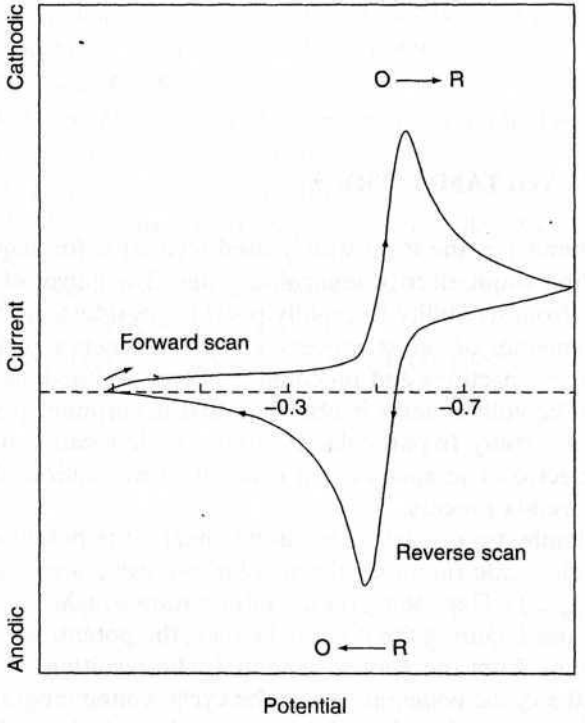

Figure 2.2 Typical cyclic voltammogram for a reversible $O + ne^- \rightleftharpoons R$ redox process.

potential approaches the characteristic E° for the redox process, a cathodic current begins to increase, until a peak is reached. After traversing the potential region in which the reduction process takes place (at least $90/n$ mV beyond the peak), the direction of the potential sweep is reversed. During the reverse scan, R molecules (generated in the forward half-cycle, and accumulated near the surface) are reoxidized back to O, resulting in an anodic peak.

The characteristic peaks in the cycle voltammogram are caused by the formation of the diffusion layer near the electrode surface. These can be best understood by carefully examining the concentration–distance profiles during the potential sweep (see Section 1.2.1.2). For example, Figure 2.3 illustrates four concentration gradients for the reactant and product at different times corresponding to (a) the initial potential value, (b,c) the formal potential of the couple (during the forward and reversed scans, respectively), and (c) the achievement of a zero-reactant surface concentration. Note that the continuous change in the surface concentration is coupled with an expansion of the diffusion-layer thickness (as expected in quiescent solutions). The resulting current peaks thus reflect the continuous change of the concentration gradient with time. Hence, the increase in the peak current corresponds to the achievement of diffusion control, while the current drop (beyond the peak)

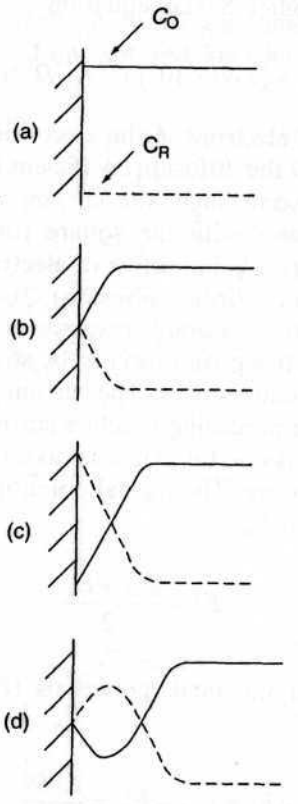

Figure 2.3 Concentration distribution of the oxidized and reduced forms of the redox couple at different times during a cyclic voltammetric experiment corresponding to the initial potential (a), to the formal potential of the couple during the forward and reversed scans (b,d), and to the achievement of a zero-reactant surface concentration (c).

exhibits a $t^{-1/2}$ dependence (independent of the applied potential). For these reasons, the reversal current has the same shape as does the forward one. As will be discussed in Chapter 4, the use of ultramicroelectrodes—for which the mass transport process is dominated by radial (rather than linear) diffusion—results in a sigmoid-shaped cyclic voltammogram.

2.1.1 Data Interpretation

The cyclic voltammogram is characterized by several important parameters. Four of these observables, the two peak currents and two peak potentials, provide the basis for the diagnostics developed by Nicholson and Shain (1) for analyzing the cyclic voltammetric response.

2.1.1.1 Reversible Systems The peak current for a reversible couple (at 25°C) is given by the Randles–Sevcik equation

$$i_p = (2.69 \times 10^5) n^{3/2} A C D^{1/2} v^{1/2} \tag{2.1}$$

where n is the number of electrons, A the electrode area (in cm^2), C the concentration (in mol/cm^3), D the diffusion coefficient (in cm^2/s), and v the potential scan rate (in V/s). Accordingly, the current is directly proportional to concentration and increases with the square root of the scan rate. Such dependence on the scan rate is indicative of electrode reaction controlled by mass transport (semiinfinite linear diffusion). The reverse-to-forward peak current ratio, $i_{p,r}/i_{p,f}$, is unity for a simple reversible couple. As will be discussed in the following sections, this peak ratio can be strongly affected by chemical reactions coupled to the redox process. The current peaks are commonly measured by extrapolating the preceding baseline current.

The position of the peaks on the potential axis (E_p) is related to the formal potential of the redox process. The formal potential for a reversible couple is centered between $E_{p,a}$ and $E_{p,c}$:

$$E^\circ = \frac{E_{p,a} + E_{p,c}}{2} \tag{2.2}$$

The separation between the peak potentials (for a reversible couple) is given by

$$\Delta E_p = E_{p,a} - E_{p,c} = \frac{0.059}{n} \text{ V} \tag{2.3}$$

Thus, the peak separation can be used to determine the number of electrons transferred, and as a criterion for a Nernstian behavior. Accordingly, a fast one-electron process exhibits a ΔE_p of about 59 mV. Both the cathodic and

anodic peak potentials are independent of the scan rate. It is possible to relate the half-peak potential ($E_{p/2}$, where the current is half of the peak current) to the polarographic half-wave potential, $E_{1/2}$:

$$E_{p/2} = E_{1/2} \pm \frac{0.028}{n} \text{ V} \tag{2.4}$$

(The sign is positive for a reduction process.)

For multielectron transfer (reversible) processes, the cyclic voltammogram consists of several distinct peaks, if the E° values for the individual steps are successively higher and are well separated. An example of such a mechanism is the six-step reduction of the fullerenes C_{60} and C_{70} to yield the hexaanion products C_{60}^{6-} and C_{70}^{6-}. Such six successive reduction peaks are observed in Figure 2.4.

The situation is very different when the redox reaction is slow or coupled with a chemical reaction. Indeed, it is these "nonideal" processes that are usually of greatest chemical interest and for which the diagnostic power of

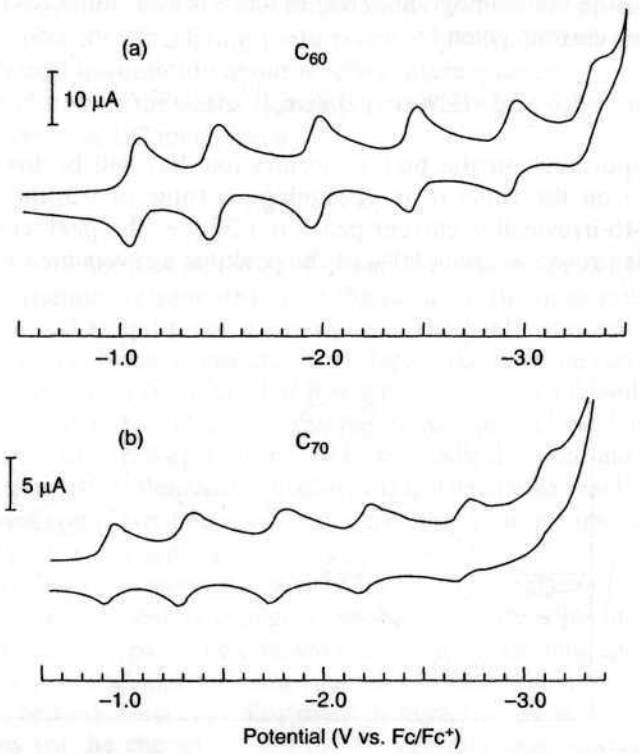

Figure 2.4 Cyclic voltammetry of C_{60} and C_{70} in an acetonitrile/toluene solution. (Reproduced with permission from Ref. 2.)

cyclic voltammetry is most useful. Such information is usually obtained by comparing the experimental voltammograms with those derived from theoretical (simulated) ones (1). Proper compensation of the ohmic drop (see Section 4.4) is crucial for such diagnostic applications of cyclic voltammetry.

2.1.1.2 Irreversible and Quasi-reversible Systems For irreversible processes (those with sluggish electron exchange), the individual peaks are reduced in size and widely separated (Fig. 2.5, curve *A*). Totally irreversible systems are characterized by a shift of the peak potential with the scan rate:

$$E_p = E^\circ - \frac{RT}{\alpha n_a F}\left[0.78 - \ln\frac{k^\circ}{D^{1/2}} + \ln\left(\frac{\alpha n_a F v}{RT}\right)^{1/2}\right] \qquad (2.5)$$

where α is the transfer coefficient and n_a is the number of electrons involved in the charge transfer step. Thus, E_p occurs at potentials higher than E°, with the overpotential related to k° and α. Independent of the value k°, such peak displacement can be compensated by an appropriate change of the scan rate. The peak potential and the half-peak potential (at 25°C) will differ by $48/\alpha n$ mV. Hence, the voltammogram becomes more drawn-out as αn decreases.

The peak current, given by

$$i_p = (2.99 \times 10^5) n(\alpha n_a)^{1/2} A C D^{1/2} v^{1/2} \qquad (2.6)$$

is still proportional to the bulk concentration, but will be lower in height (depending on the value of α. Assuming an value of 0.5, the ratio of the reversible-to-irreversible current peaks is 1.27 (i.e., the peak current for the irreversible process is about 80% of the peak for a reversible one).

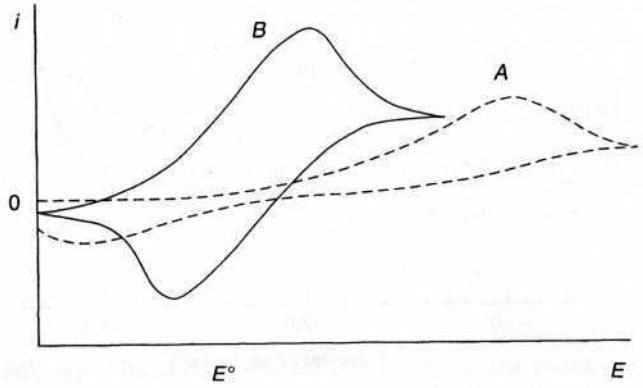

Figure 2.5 Cyclic voltammograms for irreversible (curve *A*) and quasi-reversible (curve *B*) redox processes.

For quasi-reversible systems (with $10^{-1} > k^\circ > 10^{-5}$ cm/s) the current is controlled by both the charge transfer and mass transport. The shape of the cyclic voltammogram is a function of $k^\circ/\sqrt{\pi a D}$ (where $a = nFv/RT$). As $k^\circ/\sqrt{\pi a D}$ increases, the process approaches the reversible case. For small values of $k^\circ/\sqrt{\pi a D}$ (i.e., at very fast v), the system exhibits an irreversible behavior. Overall, the voltammograms of a quasi-reversible system are more drawn out and exhibit a larger separation in peak potentials compared to a reversible system (Fig. 2.5, curve *B*).

2.1.2 Study of Reaction Mechanisms

One of the most important applications of cyclic voltammetry is for qualitative diagnosis of chemical reactions that precede or succeed the redox process (1). Such reaction mechanisms are commonly classified by using the letters E and C (for the redox and chemical steps, respectively) in the order of the steps in the reaction scheme. The occurrence of such chemical reactions, which directly affect the available surface concentration of the electroactive species, is common to redox processes of many important organic and inorganic compounds. Changes in the shape of the cyclic voltammogram, resulting from the chemical competition for the electrochemical reactant or product, can be extremely useful for elucidating these reaction pathways and for providing reliable chemical information about reactive intermediates.

For example, when the redox system is perturbed by a following chemical reaction, namely, an EC mechanism

$$O + ne^- \rightleftharpoons R \rightarrow Z \qquad (2.7)$$

the cyclic voltammogram will exhibit a smaller reverse peak (because the product R is chemically 'removed' from the surface). The peak ratio $i_{p,r}/i_{p,f}$ will thus be smaller than unity; the exact value of the peak ratio can be used to estimate the rate constant of the chemical step. In the extreme case, the chemical reaction may be so fast that all of R will be converted to Z, and no reverse peak will be observed. A classical example of such an EC mechanism is the oxidation of the drug chlorpromazine to form a radical cation that reacts with water to give an electroinactive sulfoxide. Ligand exchange reactions (e.g., of iron porphyrin complexes) occurring after electron transfer represent another example of such a mechanism.

Additional information on the rates of these (and other) coupled chemical reactions can be achieved by changing the scan rate (i.e. adjusting the experimental time scale). In particular, the scan rate controls the time spent between the switching potential and the peak potential (during which time the chemical reaction occurs). Hence, as illustrated in Figure 2.6, it is the ratio of the rate constant (of the chemical step) to the scan rate that controls the peak ratio. Most useful information is obtained when the reaction time lies within the experimental time scale. For scan rates between 0.02 and 200 V/s (common

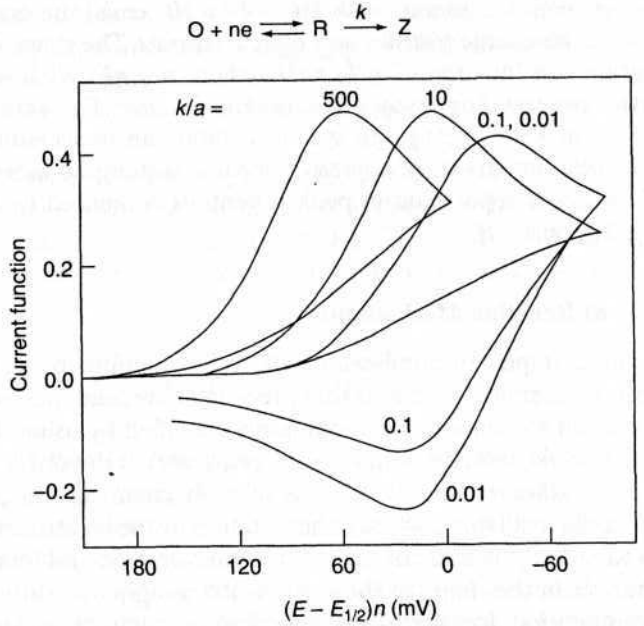

Figure 2.6 Cyclic voltammograms for a reversible electron transfer followed by an irreversible step for various ratios of chemical rate constant to scan rate k/a, where $a = nFv/RT$. (Reproduced with permission from Ref. 1.)

with conventional electrodes), the accessible time scale is around 0.1–1000 ms. Ultramicroelectrodes (discussed in Section 4.5.4) offer the use of much faster scan rates and hence the possibility of shifting the upper limit of follow-up rate constants measurable by cyclic voltammetry (3). For example, highly reactive species generated by the electron transfer, and alive for 25 ns, can be detected using a scan rate of 10^6 V/s. A wide variety of fast reactions (including isomerization and dimerization) can thus be probed. The extraction of such information commonly requires background subtraction to correct for the large charging-current contribution associated with ultrafast scan rates.

A special case of the EC mechanism is the catalytic regeneration of O during the chemical step:

$$O + ne^- \rightleftharpoons R \tag{2.8}$$

$$R + A \rightleftharpoons O \tag{2.9}$$

An example of such a catalytic EC process is the oxidation of dopamine in the presence of ascorbic acid (4). The dopamine quinone formed in the redox step is reduced back to dopamine by the ascorbate ion. The peak ratio for such a catalytic reaction is always unity.

Other reaction mechanisms can be elucidated in a similar fashion. For example, for a CE mechanism, where a slow chemical reaction precedes the electron transfer, the ratio of $i_{p,r}/i_{p,f}$ is generally larger than one, and approaches unity as the scan rate decreases. The reverse peak is seldom affected by the coupled reaction, while the forward one is no longer proportional to the square root of the scan rate.

ECE processes, with a chemical step being interposed between electron transfer steps

$$O_1 + ne^- \rightleftharpoons R_1 \rightarrow O_2 + ne^- \rightarrow R_2 \tag{2.10}$$

are also easily explored by cyclic voltammetry, because the two redox couples can be observed separately. The rate constant of the chemical step can thus be estimated from the relative sizes of the two cyclic voltammetric peaks.

Many anodic oxidations involve an ECE pathway. For example, the neurotransmitter epinephrine can be oxidized to its quinone, which proceeds via cyclization to leucoadrenochrome. The latter can rapidly undergo electron transfer to form adrenochrome (5). The electrochemical oxidation of aniline is another classical example of an ECE pathway (6). The cation radical thus formed rapidly undergoes a dimerization reaction to yield an easily oxidized *p*-aminodiphenylamine product. Another example (of industrial relevance) is the reductive coupling of activated olefins to yield a radical anion, which reacts with the parent olefin to give a reducible dimer (7). If the chemical step is very fast (in comparison to the electron transfer process), the system behaves as an EE mechanism (of two successive charge transfer steps). Table 2.1 summarizes common electrochemical mechanisms involving coupled chemical reactions. Powerful cyclic voltammetric computational simulators, exploring the behavior of virtually any user-specific mechanism have been developed (9). Such simulated voltammograms can be compared with and fitted to the experimental ones. The new software also provides "movie"-like presentations of the corresponding continuous changes in the concentration profiles.

2.1.3 Study of Adsorption Processes

Cyclic voltammetry can also be used for evaluating the interfacial behavior of electroactive compounds. Both reactant and product can be involved in an adsorption–desorption process. Such interfacial behavior can occur in studies of numerous organic compounds, as well as of metal complexes (if the ligand is specifically adsorbed). For example, Figure 2.7 illustrates repetitive cyclic voltammograms, at the hanging mercury drop electrode, for riboflavin in a sodium hydroxide solution. A gradual increase of the cathodic and anodic peak currents is observed, indicating progressive adsorptive accumulation at the surface. Note also that the separation between the peak potentials is smaller than expected for solution-phase processes. Indeed, ideal Nernstian behavior of surface-confined nonreacting species is manifested by symmetric

TABLE 2.1 Electrochemical Mechanisms Involving Coupled Chemical Reactions

1. Reversible electron transfer, no chemical complications:

$$O + ne^- \rightleftharpoons R$$

2. Reversible electron transfer followed by a reversible chemical reaction—E_rC_r mechanism:

$$O + ne^- \rightleftharpoons R$$
$$R \underset{k_{-1}}{\overset{k_1}{\leftrightarrows}} Z$$

3. Reversible electron transfer followed by an irreversible chemical reaction—E_rC_i mechanism:

$$O + ne^- \rightleftharpoons R$$
$$R \overset{k}{\leftrightarrows} Z$$

4. Reversible chemical reaction preceding a reversible electron transfer—C_rE_r mechanism:

$$Z \underset{k_{-1}}{\overset{k_1}{\leftrightarrows}} O$$
$$O + ne^- \rightleftharpoons R$$

5. Reversible chemical reaction preceding an irreversible electron transfer—C_rE_i mechanism:

$$Z \underset{k_{-1}}{\overset{k_1}{\leftrightarrows}} O$$
$$O + ne^- \rightleftharpoons R$$

6. Reversible electron transfer followed by an irreversible regeneration of starting materials—catalytic mechanism:

$$O + ne^- \rightleftharpoons R$$
$$R + Z \overset{k}{\leftrightarrows} O$$

7. Irreversible electron transfer followed by an irreversible regeneration of starting material:

$$O + ne^- \rightleftharpoons R$$
$$R + Z \overset{k}{\leftrightarrows} O$$

8. Multiple electron transfer with intervening chemical reaction—ECE mechanism:

$$O + n_1e^- \rightleftharpoons R \quad R \rightleftharpoons Y$$
$$Y + n_2e^- \rightleftharpoons Z$$

Source: Adapted with permission from Ref. 8.

cyclic voltammetric peaks ($\Delta E_p = 0$), and a peak half-width of $90.6/n$ mV (Fig. 2.8). The peak current is directly proportional to the surface coverage (Γ) and potential scan rate:

$$i_p = \frac{n^2F^2\Gamma Av}{4RT} \tag{2.11}$$

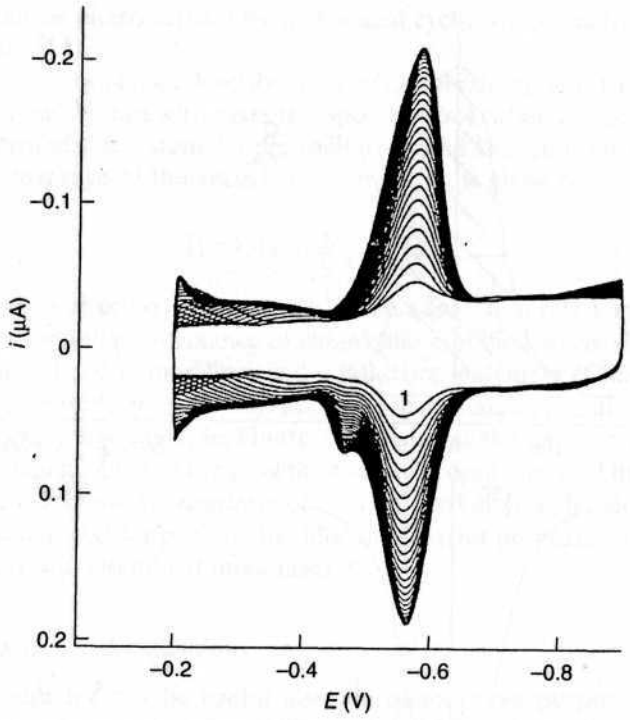

Figure 2.7 Repetitive cyclic voltammograms for 1×10^{-6} M riboflavin in a 1 mM sodium hydroxide solution. (Reproduced with permission from Ref. 10.)

Recall that a Nernstian behavior of diffusing species yields a $v^{1/2}$ dependence. In practice, the ideal behavior is approached for relatively slow scan rates, and for an adsorbed layer that shows no intermolecular interactions and fast electron transfers.

The peak area at saturation (i.e., the quantity of charge consumed during the reduction or adsorption of the adsorbed layer) can be used to calculate the surface coverage:

$$Q = nFA\Gamma \tag{2.12}$$

This can be used for calculating the area occupied by the adsorbed molecule and hence to predict its orientation on the surface. The surface coverage is commonly related to the bulk concentration via the adsorption isotherm. One of the most frequently used at present is the Langmuir isotherm

$$\Gamma = \Gamma_m \frac{BC}{1 + BC} \tag{2.13}$$

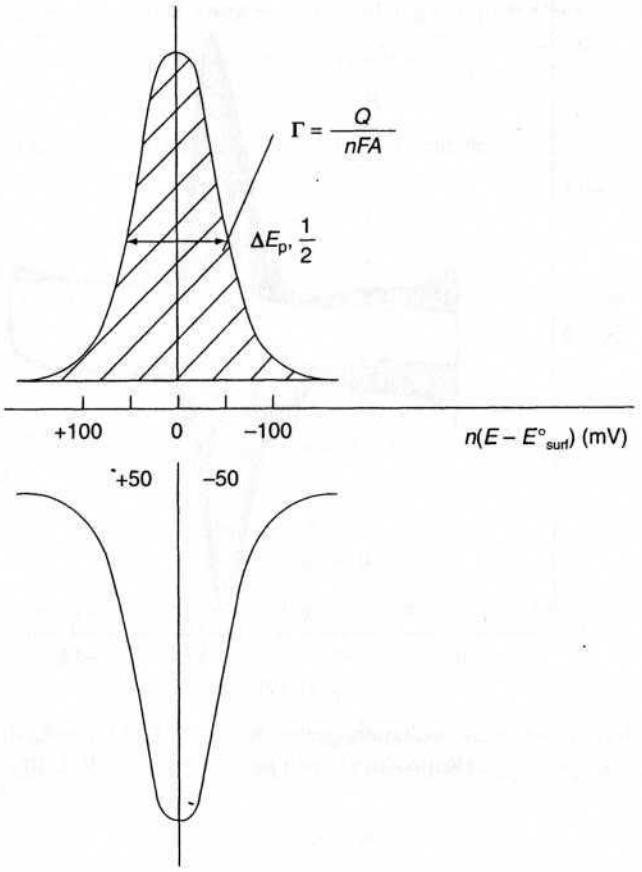

Figure 2.8 Ideal cyclic voltammetric behavior for a surface layer on an electrode. The surface coverage Γ can be obtained from the area under the peak. (Reproduced with permission from Ref. 11.)

where Γ_m is the surface concentration corresponding to a monolayer coverage (mol/cm^2) and B is the adsorption coefficient. A linearized isotherm, $\Gamma = \Gamma_m BC$, is obtained for low adsorbate concentrations (i.e., when $1 \gg BC$). The Langmuir isotherm is applicable to a monolayer coverage and assumes that there are no interactions between adsorbed species. Other isotherms (e.g., of Frumkin or Temkin) take into account such interactions. Indeed, the Langmuir isotherm is a special case of the Frumkin isotherm when no interactions exist. When either the reactant (O) or the product (R) (but not both) is adsorbed, one expects to observe a postpeak or prepeak, respectively (at potentials more negative or positive than the diffusion-controlled peak).

Equations have been derived for less ideal situations, involving quasi- and irreversible adsorbing electroactive molecules and different strengths of adsorption of the reactant and product (11–14). The rates of fast adsorption

processes can be characterized by high-speed cyclic voltammetry at ultramicroelectrodes (15).

Two general models can describe the kinetics of adsorption. The first model involves fast adsorption with mass transport control, while the other involves kinetic control of the system. Under the latter (and Langmuirian) conditions, the surface coverage of the adsorbate at time t, Γ_t, is given by

$$\Gamma_t = \Gamma_e(1 - \exp(-k'C_t t)) \tag{2.14}$$

where Γ_e is the surface coverage and k' is the adsorption rate constant.

The behavior and performance of chemically modified electrodes based on surface-confined redox modifiers and conducting polymers (Chapter 4), can also be investigated by cyclic voltammetry, in a manner similar to that for adsorbed species. For example, Figure 2.9 illustrates the use of cyclic voltammetry for in situ probing of the growth of an electropolymerized film. Changes in the cyclic voltammetric response of a redox marker (e.g., ferrocyanide) are commonly employed for probing the blocking/barrier properties of insulating films (such as self-assembled monolayers).

2.1.4 Quantitative Applications

Cyclic voltammetry can be useful also for quantitative purposes, based on measurements of the peak current [Eq. (2.1)]. Such quantitative applications

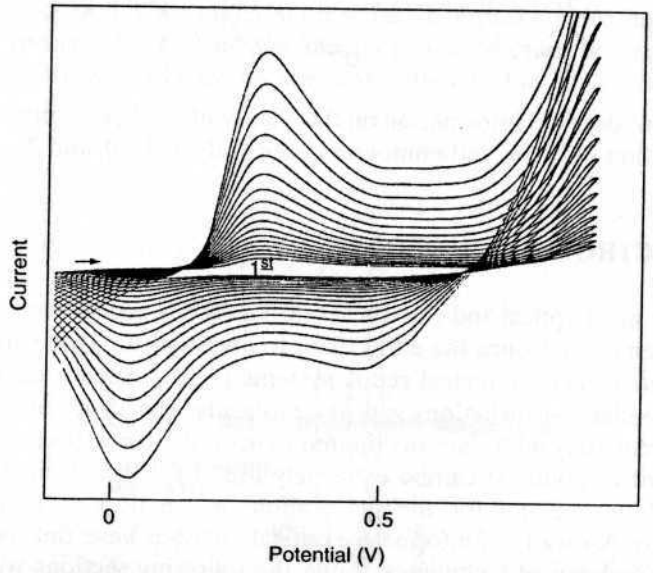

Figure 2.9 Repetitive cyclic voltammograms illustrating the continuous growth of polyaniline on a platinum surface.

require the establishment of the proper baseline. For neighboring peaks (of a mixture), the baseline for the second peak is obtained by extrapolating the current decay of the first one (in accordance to $t^{-1/2}$). Background reactions, primarily those associated with the double-layer charging and redox surface processes, limit the detection limit to around the 1×10^{-5} M level. Background-subtracted cyclic voltammetry can be employed for measuring lower concentrations (16). In particular, fast-scan (500–1000-V/s) background-subtracted cyclic voltammetry at carbon fiber microelectrodes is seeing increased use for the in vivo monitoring of neurotransmitters (such as dopamine or serotonin) in the human brain (17). Such coupling of digital background subtraction and fast voltammetric measurements provides the subsecond temporal resolution necessary for detecting dynamic concentration changes in the micromolar range occurring in the extracellular environment of the brain. The good temporal and chemical resolutions of such in vivo cyclic voltammetric experiments offer improved understanding of the chemistry of the brain. These repetitive scanning in vivo experiments generate large quantities of data, which are best represented as three-dimensional (potential, current, time) color contour images (18). For example, the temporal release of dopamine following an electrical stimulation is evidenced from the rapid increase in color around its peak potential. The ultrafast scanning also eliminates interferences from adsorption processes and chemical reactions that are coupled to the primary oxidation reaction of catecholamine neurotransmitters (19):

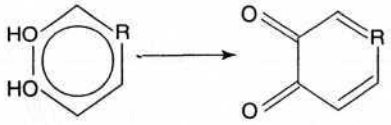

$$+ 2H^+ + 2e^- \qquad (2.15)$$

For more detailed information on the theory of cyclic voltammetry, and the interpretation of cyclic voltammograms, see Refs. 1, 7, 20, and 21.

2.2 SPECTROELECTROCHEMISTRY

The coupling of optical and electrochemical methods, spectroelectrochemistry, has been employed since the early 1980s to investigate a wide variety of inorganic, organic, and biological redox systems (22,23). Such a combination of electrochemical perturbations with the molecular specificity of optical monitoring successfully addresses the limited structural information available from the current response. It can be extremely useful for the elucidation of reaction mechanisms, and for the delineation of kinetic and thermodynamic parameters. A variety of informative optical methods have thus been coupled with electrochemical techniques. While the following sections will focus primarily on transmission absorption UV–vis (ultraviolet–visible) spectroscopic procedures, powerful spectroelectrochemical data can be obtained in reflectance experiments (in which the light beam is reflected from the electrode surface), using vibrational spectroscopic investigations, as well as from luminescence and scattering spectrochemical studies.

2.2.1 Experimental Arrangement

Optically transparent electrodes (OTEs), which enable light to be passed through their surface and the adjacent solution, are the key for performing transmission spectroelectrochemical experiments. One type of OTE consists of a metal (gold, silver, nickel) micromesh containing small (10–30-μm) holes, which couples good optical transmission (over 50%) with good electrical conductivity. Such a minigrid is usually sandwiched between two microscopic slides, which form a thin-layer cell (Fig. 2.10). The resulting chamber, containing the electroactive species in solution, contacts a larger container that holds the reference and auxiliary electrodes. The OTE is placed in the spectrophotometer so that the optical beam is passed directly through the transparent electrode and the solution. The working volume of the cell is only 30–50 μL, and complete electrolysis of the solute requires only 30–60 s. Alternately, the OTE may consist of a thin (100–5000-Å) film of a metal (e.g., gold, platinum) or a semiconductor (e.g., tin oxide), deposited on a transparent material such as quartz or glass substrate. The film thickness is often selected as a compromise between its electrical conductivity and optical transmission.

Improvements in cell design have been reported, including the use of fiber optics for the illumination and collection of light near electrode surfaces (24), the fabrication of long-pathlength OTEs via drilling of a small hole through a solid conducting material for sensitive optical monitoring of weakly absorbing species (25,26), and the incorporation of open porous materials (particularly reticulated vitreous carbon) within a thin-layer compartment (27).

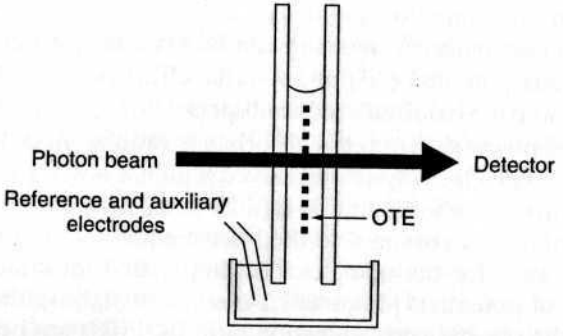

Figure 2.10 Thin-layer spectroelectrochemical cell.

2.2.2 Principles and Applications

The primary advantage of spectroelectrochemistry is the cross-correlation of information from the simultaneous electrochemical and optical measurements. In a typical experiment, one measures absorption changes resulting from species produced (or consumed) in the redox process. The change in absorbance is related to concentration and optical path length. Careful evaluation of the temporal absorbance response (A–t curve) during the electrochemical generation (or consumption) of an optically active species can yield extremely useful insight on reaction mechanisms and kinetics. Such experiments are particularly useful when the reactant and product have sufficiently different spectra.

Consider, for example, the general redox process:

$$O + ne^- \rightleftharpoons R \tag{2.16}$$

When the potential of the OTE is stepped to a value such that reaction (2.16) proceeds at a diffusion-controlled rate, the time-dependent absorbance of R is given by

$$A = \frac{2C_O\varepsilon_R D_O^{1/2} t^{1/2}}{\pi^{1/2}} \tag{2.17}$$

where ε_R is the molar absorptivity of R and D_O and C_O are the diffusion coefficient and concentration of O, respectively. Hence, A increases linearly with the square root of time ($t^{1/2}$), reflecting the continuous generation of R at a rate determined by the diffusion of O to the surface. Equation (2.17) is valid when the generated species is stable. However, when R is a short-lived species (i.e., an EC mechanism), the absorbance response will be smaller than that expected from Eq. (2.17). The rate constant for its decomposition reaction can thus be calculated from the decrease in absorbance. Many other reaction mechanisms can be studied in a similar fashion from the deviation of the A–t curve from the shape predicted by Eq. (2.17). Such a potential-step experiment is known as *chronoabsorptometry*.

Thin-layer spectroelectrochemistry can be extremely useful for measuring the formal redox potential ($E°$) and n values. This is accomplished by spectrally determining the oxidized : reduced species concentration ratio ([O]/[R]) at each applied potential (from the absorbance ratio at the appropriate wavelengths). Since bulk electrolysis is achieved within a few seconds (under thin-layer conditions), the whole solution rapidly reaches an equilibrium with each applied potential (in accordance to the Nernst equation). For example, Figure 2.11 shows spectra for the complex $[Tc(dmpe)_2Br_2]^+$ in dimethylformamide using a series of potentials [dmpe is 1,2-bis(dimethylphosphine) ethane]. The logarithm of the resulting concentration ratio ([O]/[R]) can be plotted against the applied potential to yield a straight line, with an intercept corresponding

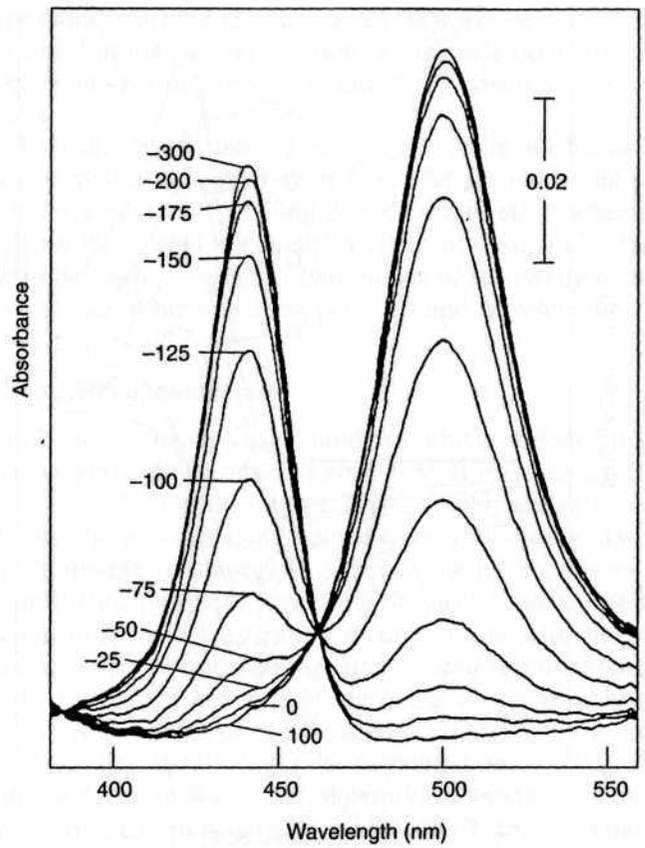

Figure 2.11 Spectra for a series of applied potentials (mV vs. Ag/AgCl) during thin-layer spectroelectrochemical experiment on 1.04×10^{-3}M $[Tc(III)(dmpe)_2Br_2]^+$. Medium: DMF containing 0.5 M TEAP. (Reproduced with permission from Ref. 28.)

to the formal potential. The slope of this Nernstian plot (0.059/n V) can be used to determine the n value.

Besides potential-step experiments, it is possible to employ linear potential scan perturbations of an OTE (28). This voltabsorptometric approach results in an optical analog of a voltammetric experiment. A dA/dE–E plot (obtained by differentiating the absorbance of the reaction product with respect to the changing potential) is morphologically identical to the voltammetric response for the redox process (Fig. 2.12). Depending on the molar absorptivity of the monitored species, the derivative optical response may afford a more sensitive tool than the voltammetric one. This concept is also not prone to charging-current background contributions and holds considerable promise for mechanism diagnosis and kinetic characterization of coupled chemical reactions.

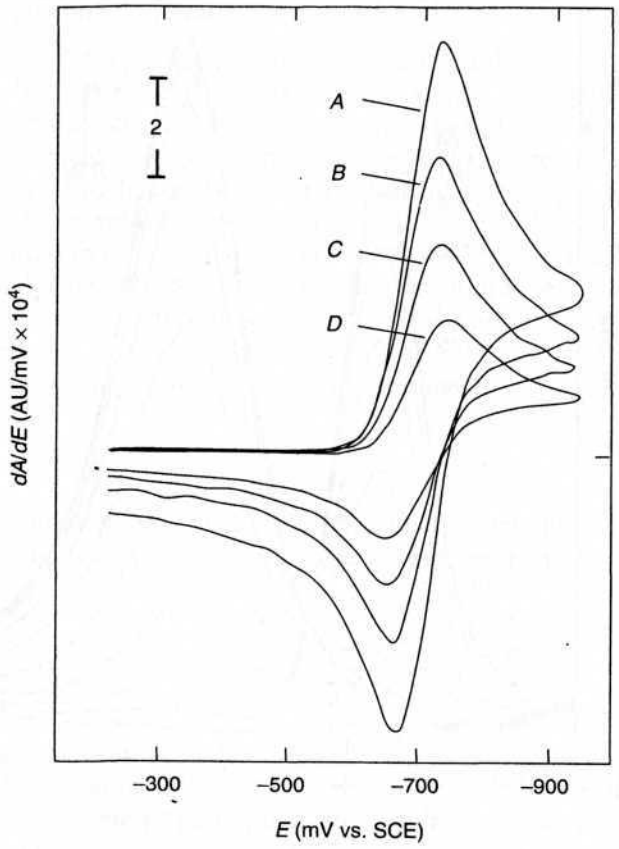

Figure 2.12 Plot of dA/dt versus E for 1.55×10^{-3} M methyl viologen at tin oxide OTE, using scan rates of 25 (A), 50 (B), 97.2 (C), and 265 (D) mV/s. (Reproduced with permission from Ref. 29.)

Spectroelectrochemical experiments can be used to probe various adsorption and desorption processes. In particular, changes in the absorbance accrue from such processes can be probed utilizing the large ratio of surface area to solution volume of OTEs with long optical pathlength (30). Additional information on such processes can be attained from the Raman spectroelectrochemical experiments described below.

In addition to transmission experiments, it is possible to use more sensitive reflectance protocols. In particular, in internal reflectance spectroscopy (IRS) the lightbeam is introduced to the electrode at an angle, and the spectrum are recorded from the reflected beam at the solid–solution interface. Prisms are used to let the radiation enter and leave. Besides its higher sensitivity, IRS is less prone to solution resistance effects.

Infrared spectroelectrochemical methods, particularly those based on Fourier transform infrared (FTIR), can provide structural information that

UV–vis absorbance techniques do not. FTIR spectroelectrochemicstry has thus been fruitful in the characterization of reactions occurring on electrode surfaces. The technique requires very thin cells to overcome solvent absorption problems.

Besides its widespread use for investigating the mechanism of redox processes, spectroelectrochemistry can be useful for analytical purposes. In particular, the simultaneous profiling of optical and electrochemical properties can enhance the overall selectivity of different sensing (31) and detection (32) applications. Such coupling of two modes of selectivity is facilitated by the judicious choice of the operating potential and wavelength.

2.2.3 Electrochemiluminescence

Electrochemiluminescence (ECL) is another useful technique for studying the fate of electrogenerated radicals that emit light. It involves the formation of light-emitting excited-state species as a result of highly and fast energetic electron transfer reactions of reactants formed electrochemically (33–36). Various organic and inorganic substances [e.g., polycyclic hydrocarbons, nitro compounds, luminol, $Ru(bpy)_3^{2+}$] can produce ECL on electron transfer from electrodes, in connection to the formation of radical ions. The electrogenerated radicals behave as very strong redox agents, and their reactions with each other or with other substances are sufficiently energetic to be able to populate excited states. ECL experiments are usually carried out by recording the spectra of the emitted light using a deoxygenated nonaqeous medium (e.g., highly purified acetonitrile or DMF). Operation in nonaqeous medium commonly involves the $Ru(bpy)_3^{2+}$ label because its ECL can be generated in this medium.

Analytical applications of ECL—relying on the linear dependence of the ECL light intensity and the reactant concentration—have also been realized (37). Since very low light levels can be measured (e.g., by single-photon counting methods), ECL offers extremely low detection limits. Such remarkable sensitivity has been exploited for a wide range of ECL-based immunoassays or DNA bioassays based on a $Ru(bpy)_3^{2+}$ label along with the tripropylamine (TPA) reagent (38). In order to generate light, $Ru(bpy)_3^{2+}$ and TPA are oxidized at the electrode surface to form a strong oxidant $Ru(bpy)_3^{3+}$ and a cation radical TPA^{+*}, respectively. The latter loses a proton and react with $Ru(bpy)_3^{3+}$ to form an excited state of $Ru(bpy)_3^{2+}$, which decays while releasing a photon at 620 nm (Fig. 2.13). The use of ECL as a detection method for liquid chromatography and microchip devices has also been documented (39,40).

In addition to UV–vis absorption measurements, other spectroscopic techniques can be used for monitoring the dynamics of electrochemical events or the fate of electrogenerated species. Particularly informative are the couplings of electrochemistry with electron spin resonance, nuclear magnetic resonance, and mass spectroscopy. A variety of specially designed cells have been con-

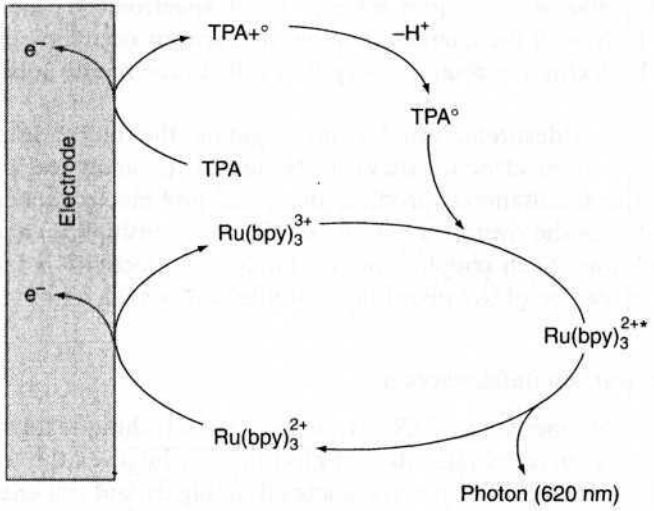

Figure 2.13 Electrochemiluminescence (ECL) reaction sequence, based on a $Ru(bpy)_3^{2+}$ label, commonly used for immunoassays or DNA bioassays.

structed to facilitate such studies, and several reviews have been published (41–45).

2.2.4 Optical Probing of Electrode–Solution Interfaces

Additional spectroscopic techniques can be used for probing the molecular structure of electrode–solution interfaces, as desired for understanding the fundamentals of electrode surfaces. The focus of these surface techniques is the correlation of the surface structure with electrochemical reactivity. Such surface-sensitive analytical tools can be classified as in situ or ex situ. In particular, the high sensitivity of molecular vibrations to the chemical environment has led to the widespread use of vibrational spectroscopies, such as surface-enhanced Raman scattering (SERS) for monitoring the surface composition before, during, and after the electrochemical experiment. In these experiments, a small fraction of the photons exchanges energy with the sample and are inelastically scattered, with a change of their wavelength characteristic of the energy change. Such Raman scattering effect can be enhanced by factors of $\leq 10^8$ when the compound is adsorbed on metal surfaces (46). The enhancement process is believed to result from the combination of several electromagnetic and chemical effects between the molecule and the metal surface. Since this scattering efficiency increases dramatically in the adsorbate state, Raman spectroelectrochemistry has been used primarily for investigating species adsorbed on electrodes (47). Another powerful in situ structural characterization technique, *X-ray adsorption fine structure* (EXAFS), refers to the modulation in the X-ray adsorption coefficient beyond the adsorption

edge. Readers interested in these in situ techniques are referred to a 1991 monograph (48). Scanning electron microscopy (SEM) represents another widely used technique for obtaining ex situ information on the surface morphology and chemical composition (see, e.g., Fig. 4.20).

Other powerful ex situ techniques are based on the detection of charged particles derived from or interacting with the surface. Among these are low-energy electron diffraction (LEED), Auger electron spectroscopy (AES), and X-ray photoelectron spectroscopy (XPS), which are carried out in ultrahigh vacuum (UHV). In LEED, electrons directed at the sample at low energies (20–200 eV) diffract to produce a pattern unique to each substrate and adsorbed layer. In AES, an electron bombardment creates a vacancy in the electronic level close to the nucleus. This vacancy is filled by an electron coming from another electronic level, with the excess energy dissipated through ejection of a secondary electron (an Auger electron). The resulting energy spectrum consists of Auger peaks that are unique to each element. XPS [also known as *electron spectroscopy for chemical analysis* (ESCA)] can also provide atomic information about the surface region. In this technique, electrons are emitted from the sample on its irradiation with monochromatic X rays. The photon energy is related to the ionization (binding) energy E_B, the energy required to remove the electron from the initial state. Most elements (with the exception of hydrogen and helium) produce XPS signals with distinct E_B. In view of the limited penetration of X rays into solids, the technique gives useful information about surface structures or layers. The appearance of new XPS peaks can thus be extremely useful for studies of modified electrodes. The reliability of information gained by such ex situ analysis depends on a knowledge of what happens during vacuum exposure. Uncertainties associated with potential loss of material during such exposure have led to renew emphasis on direct (in situ) probes.

2.3 SCANNING PROBE MICROSCOPY

The more recently developed scanning probe microscopies (SPMs) appear to revolutionize the understanding of electrode processes. The purpose of this family of microscopes is to acquire high-resolution data of surface properties. The various scanning probe microscopies have similar subcomponents but different sensing probes. These high-resolution microscopies rely on sensing the interactions between a probe tip and the target surface, while scanning the tip across the surface. Different types of interactions can be sensed by the tip to yield different imaging signals. Such signals are displayed as gray scale portraits, reflecting the extent of the tip–surface interaction. With microcomputers, the image processing becomes possible in very short times. Among the various scanning probe microscopies, scanning tunneling microscopy, atomic force microscopy, and scanning electrochemical microscopy have been useful for imaging electrode surfaces directly (under potential control), and have thus

dramatically improved the understanding of electrode reactions. Scanning probe microscopes have also been useful for creating nanostructures, through patterned movement and arrangement of nanoparticles and selected molecules.

2.3.1 Scanning Tunneling Microscopy

Scanning tunneling microscopy (STM) has revolutionized the field of surface science by allowing the direct imaging of surfaces on the atomic scale. The scanning tunneling microscope consists of a very sharp metallic tip that is moving over the surface of interest with a ceramic piezoelectric translator. The basis for its operation is the electron tunneling between the metal tip and the sample surface. The tunneling current (i_t) that flows when a voltage is applied between the sample and the tip is extremely sensitive to the sample–tip separation. In the simplest one-dimensional treatment i_t is given by

$$i_t \alpha \exp\left[(-4S\pi/h)(2m\phi)^{1/2}\right] \tag{2.18}$$

where S is the barrier width (equivalent to the shortest distance between the sample surface and the end of the tip), h is Planck's constant, m is the electron mass, and ϕ is the barrier height (equivalent to the local work function). In practice, i_t can change by a factor of ≥2 with a change of the tip–sample separation of only 1 Å. Accordingly, i_t tends to vary with the sample topography.

Although much of the early STM work has focused on investigating surfaces in vacuum, more recent work has demonstrated that surface images can also be obtained in liquid and air. In particular, the STM probing of electrode–electrolyte interfaces has attracted considerable attention (49–51). The ability of STM to offer structural information at the atomic level makes it highly suitable for in situ studies of time-dependent electrochemical processes, such as corrosion, electrodeposition, and adsorption, as well as surface modification, passivation, and activation. For example, Figure 2.14 shows a representative three-dimensional STM view of an electrochemically pretreated glassy carbon electrode, while Figure 2.15 illustrates an STM image of a spontaneously adsorbed alkanethiol monolayer on a gold surface. Useful insights into the structural–preparation relationships of conducting polymers can also be achieved by monitoring the growth of such films under different conditions (54). In addition to topographic information, the high sensitivity of the tunneling current to changes in the local work function (i.e., surface conductivity) offers a distinct visualization of composite electrode surfaces (55).

The more recent introduction of commercial STMs incorporating a potentiostat and an electrochemical cell has greatly facilitated in situ investigations of electrochemical processes. A block diagram of such STM–electrochemical system is shown in Figure 2.16. Coupled with powerful software, such instruments allow the simultaneous acquisition and display of the electrochemical

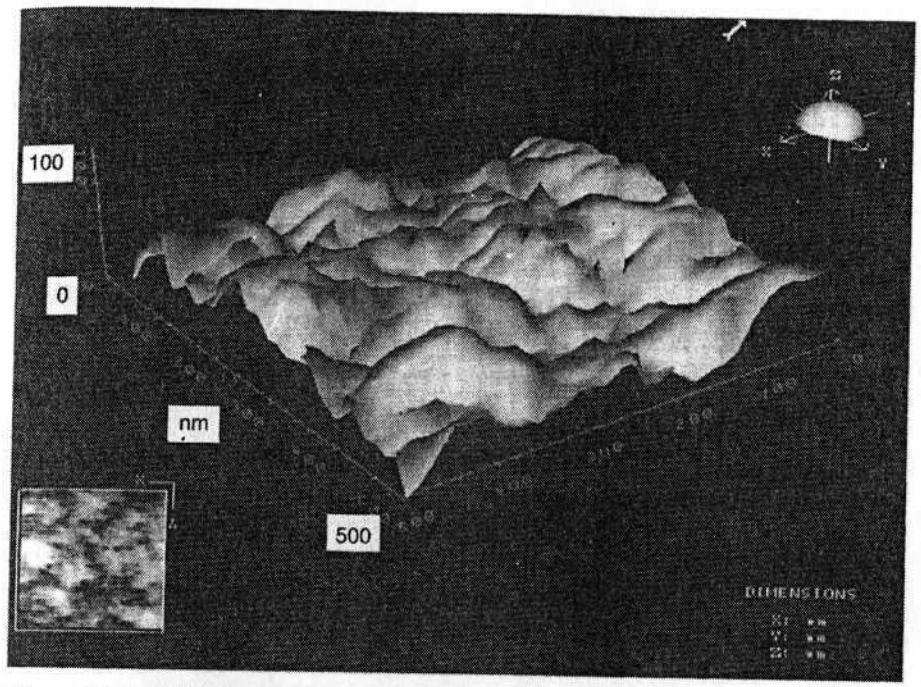

Figure 2.14 STM image of an electrochemically activated glassy carbon surface. (Reproduced with permission from Ref. 52.)

and topographic data. Extremely useful insights can thus be obtained by correlating the surface microstructures and the electrochemical reactivity. The interpretation of STM images requires extreme caution, and the tip should be shielded properly (from the electrolyte) to minimize the stray capacitance. Yet, the powerful coupling of STM and electrochemical systems offers many exciting future opportunities.

2.3.2 Atomic Force Microscopy

Atomic force microscopy (AFM) has become a standard technique to image with high resolution the topography of surfaces. It enables one to see nanoscopic surface features while the electrode is under potential control. This powerful probe microscopy operates by measuring the force between the probe and the samples (56,57). The probe consists of a sharp tip (made of silicon or silicon nitride) attached to a force-sensitive cantilever. The tip scans across the surface (by a piezoelectric scanner), and the cantilever deflects in response to force interactions between the tip and the substrate. Such deflection is monitored by bouncing a laser beam off it onto a photodetector. The measured force is attributed to repulsion generated by the overlap of the electron cloud at the probe tip with the electron cloud of surface atoms.

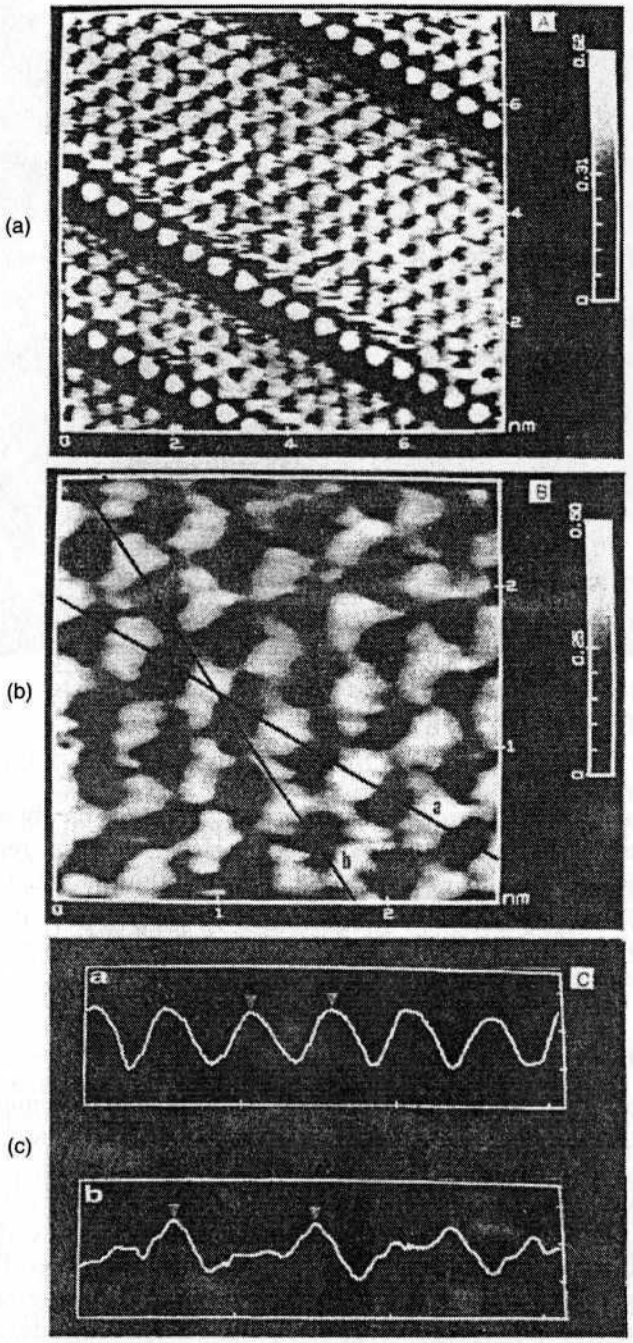

Figure 2.15 STM image of 7.7 × 7.7-nm (a) and 2.65 × 2.65-nm (b) sections of an ethanethiolate monolayer on a gold film; (c) contours of the image along the lines *a* and *b* in panel (b). (Reproduced with permission from Ref. 53.)

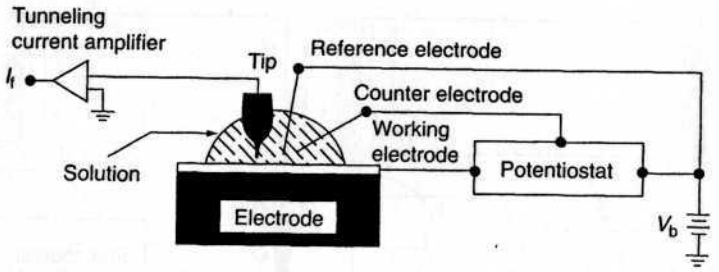

Figure 2.16 Design of a system for in situ electrochemical scanning tunneling microscopy.

It depends in part on the nature of the electrode, the distance between the electrode and the tip, any surface contamination, and the tip geometry. An image (revealing individual atoms) is created as the probe is translated across the surface, while sensing the interaction of the force fields by the cantilever beam. Such images can be formed by a constant force or height modes (with known or measured deflections of the cantilever, respectively). Since AFM does not involve passage of current between the tip and the surface, it is useful for exploring both insulating and conducting regions. The surface structure of a wide range of materials can thus be explored, irrespective of their conductivity. The technique has thus been extremely useful for observing changes in electrode surfaces caused by adsorption, etching, or underpotential deposition. Note, however, that in its conventional form, AFM lacks chemical specificity. The topographic imaging capability of AFM has been shown useful for monitoring changes in the height associated with ligand–receptor binding events (such as antibody–antigen recognition), indicating promise for label-free biochips (58). In addition to imaging applications, atomic force probes have found important applications ranging from dip-pen nanolithography (59) to microcantilever-based sensors (60). The former allows depositing "inks" (such as biomolecules) onto solid surfaces in high resolution with the AFM tip used as a "pen".

2.3.3 Scanning Electrochemical Microscopy

The scanning tunneling microscope (STM) has led to several other variants (61). Particularly attractive for electrochemical studies is scanning electrochemical microscopy (SECM) (62–65). In SECM, faradaic currents at an ultramicroelectrode tip are measured while the tip is moved (by a piezoelectric controller) in close proximity to the substrate surface that is immersed in a solution containing an electroactive species (Fig. 2.17). These tip currents are a function of the conductivity and chemical nature of the substrate, as well as of the tip–substrate distance. The images thus obtained offer valuable insights into the microdistribution of the electrochemical and chemical activity, as well

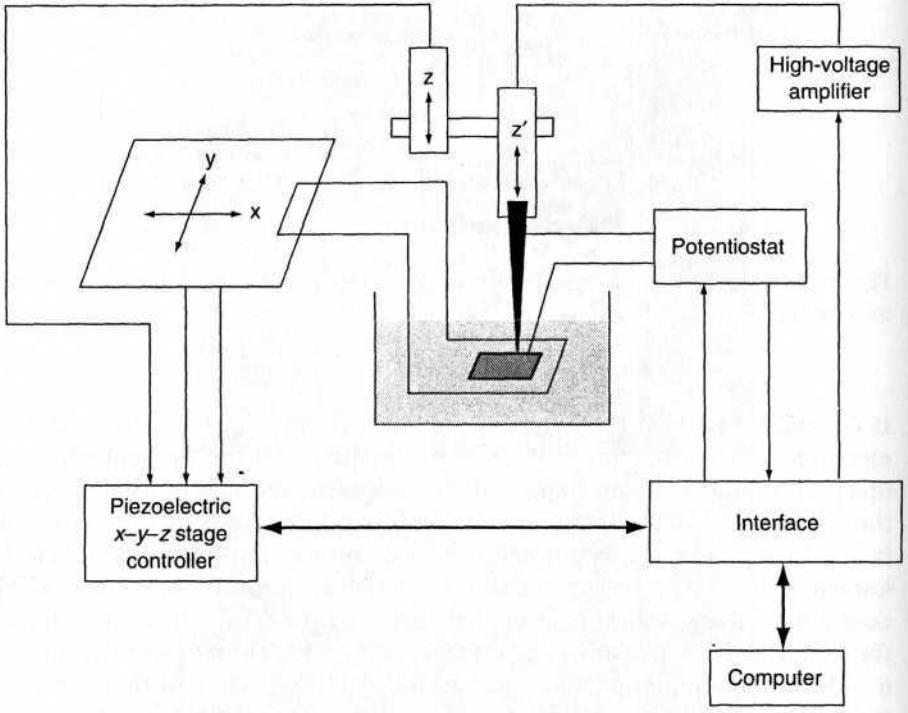

Figure 2.17 Design of a scanning electrochemical microscope. (Reproduced with permission from Ref. 66.)

as the substrate topography. A wide range of important applications involving different electrochemical systems have thus been developed.

The most common version of SECM, the feedback mode, involves recycling of an electroactive material between the tip and substrate surfaces (Fig. 2.18). When the microelectrode is distant from the surface by several electrode diameters, a steady-state current $i_{T,\infty}$ is observed at the tip (Fig 2.18a). When the tip is brought near a conductive substrate (held at sufficiently positive potential), the tip-generated product R can be oxidized back to O, and the tip current will be greater than $i_{T,\infty}$ (Fig. 2.18b). In contrast, when the tip passes over an insulating region (on the substrate), diffusion to the tip is hindered, and the feedback current diminishes (Fig. 2.18c). For example, Figure 2.19 displays a two-dimensional scan of a gold minigrid surface. The conducting gold lines are clearly observed from the enhanced recycling current. Alternately, in the collection mode, the tip is used only as a detector of species generated at the substrate. The distribution of the electrochemical activity of the surface can thus be mapped. The submicron resolution of SECM images is controlled by the size and shape of the tip, and it can be further improved by using digital image processing techniques. Yet, unlike STM or AFM, atomic resolution

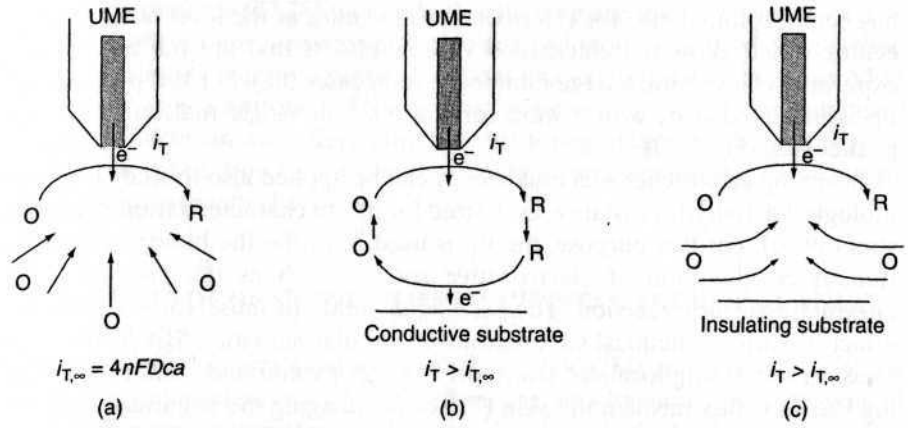

Figure 2.18 Principles of SECM: (a) tip far from the substrate surface; diffusion of O leads to steady-state current; (b) tip near a conductive substrate, with positive feedback of O; (c) tip near the insulating substrate; hindered diffusion of O. (Reproduced with permission from Ref. 65.)

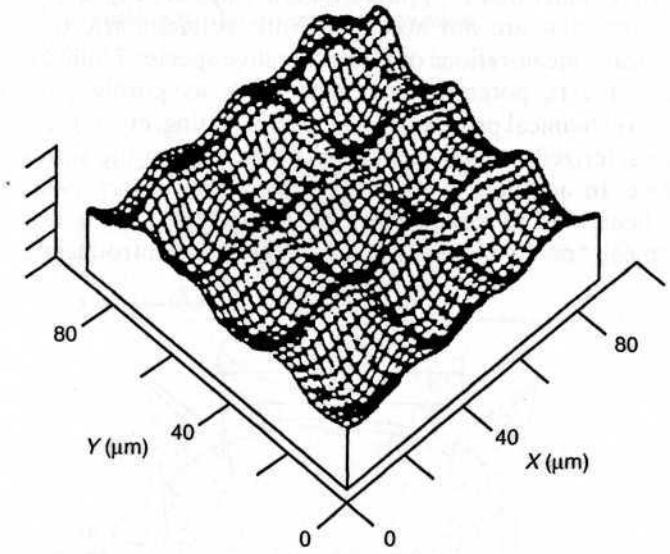

Figure 2.19 SECM image of a gold minigrid surface. (Reproduced with permission from Ref. 67.)

cannot be attained in SECM. Scanning electrochemical microscopy can also be used to investigate heterogeneous reaction kinetics. This is accomplished by forming a twin-electrode thin layer between the tip and a conducting substrate. Such configuration induces high rates of mass transfer and leads to tip currents limited by the intrinsic electron transfer rates. The volume reduction

has been exploited also for electrochemical studies at the level of single molecules, which allow the elucidation of new effects that are not apparent in experiments involving a large number of molecules (68). For this purpose, the tip is insulated (e.g., with a wax) for trapping the single molecule in a tiny pocket (e.g., Fig. 2.20).

Scanning electrochemical microscopy can be applied also to study localized biological activity, for instance, as desired for in situ characterization of biosensors (69,70). For this purpose, the tip is used to probe the biological generation or consumption of electroactive species, such as the product of an enzymatic surface reaction. The technique holds promise for studying the effect of various chemical stimulations on cellular activities. SECM has been used for measuring localized transport through membranes, such as monitoring the ionic flux through the skin (71) or for imaging the respiratory activity single living cells, for instance, through measurements of oxygen at the sensing probe (72), or for visualizing DNA duplex spot regions of DNA microarrays (73).

The utility of potentiometric (pH-selective) tips has also been documented for imaging pH profiles, including those generated by enzymatic (urease) reactions (74). These and other (75) potentiometric tips are expected to probe different reactions that are not accessible with voltammetric tips, such as to determine local concentrations of electroinactive species. Unlike their voltammetric counterparts, potentiometric tips serve as purely passive sensors. Various electrochemical processes (e.g., electroplating, etching, corrosion) can also be characterized at high resolution while moving the tip over the substrate surface. In addition to its extensive use for surface characterization, SECM has been used as a microfabrication tool (76), with its tip acting as an electrochemical "pen" or "eraser." More recently introduced commercial

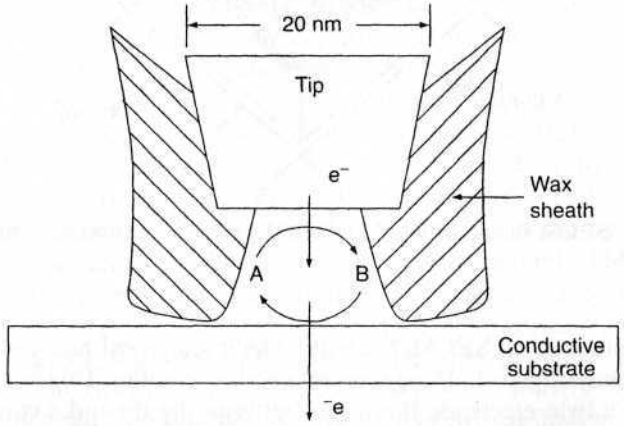

Figure 2.20 Single-molecule detection with SECM. Molecule A is trapped between the tip and the surface. (Reproduced with permission from Ref. 68.)

SECM instruments (77,78) will undoubtedly increase the scope and power of SECM. Further improvements in the power and scope of SECM has resulted from its coupling scanning probe or optical imaging techniques, such as AFM (57,79) or single-molecule fluorescence spectroscopy (80). The combined SECM-AFM technique offers simultaneous topographic and electrochemical imaging in connection to a probe containing a force sensor and an electrode component, respectively.

2.4 ELECTROCHEMICAL QUARTZ CRYSTAL MICROBALANCE

Electrochemical quartz crystal microbalance (EQCM) is a powerful tool for elucidating interfacial reactions based on the simultaneous measurement of electrochemical parameters and mass changes at electrode surfaces. The microbalance is based on a quartz crystal wafer, which is sandwiched between two electrodes, used to induce an electric field (Fig. 2.21). Such a field produces a mechanical oscillation in the bulk of the wafer. Surface reactions, involving minor mass changes, can cause perturbation of the resonant frequency of the crystal oscillator. The frequency change (Δf) relates to the mass change (Δm) according to the *Sauerbrey equation*:

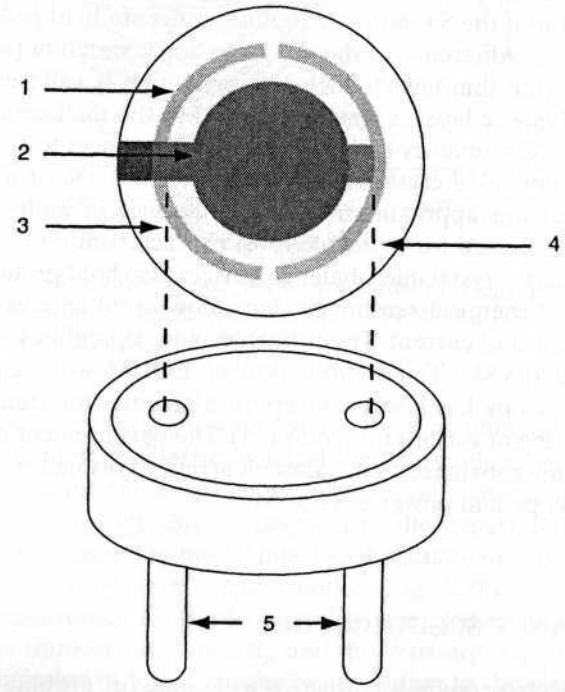

Figure 2.21 Quartz crystal microbalance: (1) the quartz crystal; (2) the gold electrode; (3,4) connecting metal wires; (5) the base.

$$\Delta f = -2\Delta mn f_0^2 / A\sqrt{\mu\rho} \qquad (2.19)$$

where n is the overtone number, f_0 the base resonant frequency of the crystal (prior to the mass change), A is the area (cm^2), μ is the shear modulus of quartz ($2.95 \times 10^{11}\,g\,cm^{-1}\,s^{-1}$), and ρ is the density of quartz ($2.65\,g/cm^3$). As expected from the negative sign, decreases in mass correspond to increases in frequency and vice versa. The Sauebrey equation forms the basis for the excellent mass sensitivity of the EQCM. In situ mass changes of $1\,ng/cm^2$ can thus be detected. The EQCM is very useful for probing processes that occur uniformly across the surface. Numerous surface reactions have thus been investigated, including deposition or dissolution of surface layers and various uptake processes (such as doping/undoping of conducting polymers or ion exchange reactions at polymer films). Such changes can be probed using various controlled-potential or controlled-current experiments. In these experiments, one of the electrodes (on the wafer) contacts the solution and serves as the working electrode in the electrochemical cell, to allow simultaneous frequency and current measurements. For example, Figure 2.22 displays the frequency (mass) vs. potential profiles, and the corresponding cyclic voltammograms, during the uptake of a multiply charged complex ion at an ion exchanger coated electrode. Other useful examples of probing the uptake of mobile species by polymer-coated electrodes were given by Hillman et al. (82). Application of the Sauerbrey equation to the study of polymeric films in solutions requires adherence to the rigid-film approximation (i.e., behavior of elastic, solvent-free thin layer). Such approximation is valid when the thickness of the polymeric layer is small compared to the thickness of the crystal, and the measured frequency change is small with respect to the resonant frequency of the unloaded crystal. Mass changes of ≤0.05% of the crystal mass commonly meet this approximation. In the absence of molecular specificity EQCM cannot be used for molecule-level characterization of surfaces. Electrochemical quartz crystal microbalance devices also hold promise for the task of affinity-based chemical sensing, as they allow simultaneous measurements of both the mass and current. The principles and capabilities of EQCM have been reviewed (83,84). The combination of EQCM with scanning electrochemical microscopy has also been reported recently for studying the dissolution and etching of various thin films (85). The development of multichannel quartz crystal microbalance (86), based on arrays of resonators, should further enhance the scope and power of EQCM.

2.5 IMPEDANCE SPECTROSCOPY

Impedance spectroscopy is an effective technique for probing the features of chemically-modified electrodes and for understanding electrochemical reaction rates (87,88). Impedance is the totally complex resistance encountered

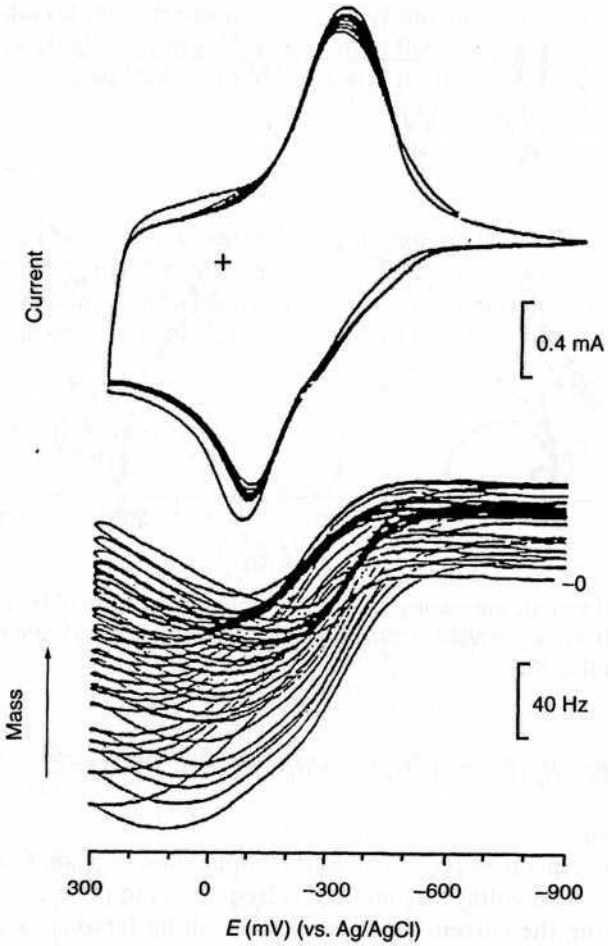

Figure 2.22 EQCM (bottom) and cyclic voltammetry (top) profiles at an ion-exchanger-coated electrode in the presence of 6×10^{-3} M $Ru(NH_3)_6Cl_6$. (Reproduced with permission from Ref. 81.)

when a current flows through a circuit made of combinations of resistors, capacitors, or inductors. Electrochemical transformations occurring at the electrode–solution interface can be modeled using components of the electronic equivalent circuitry that correspond to the experimental impedance spectra. Particularly useful to model interfacial phenomena is the Randles and Ershler electronic equivalent-circuit model (Fig. 2.23). This includes the double-layer capacitance C_d, the ohmic resistance of the electrolyte solution R_s, the electron transfer resistance R_p, and the Warburg impedance W resulting from the diffusion of ions from the bulk solution to the electrode surface. The impedance of the interface, derived by application of Ohm's law, consists of two parts, a real number Z′ and an imaginary one, Z″:

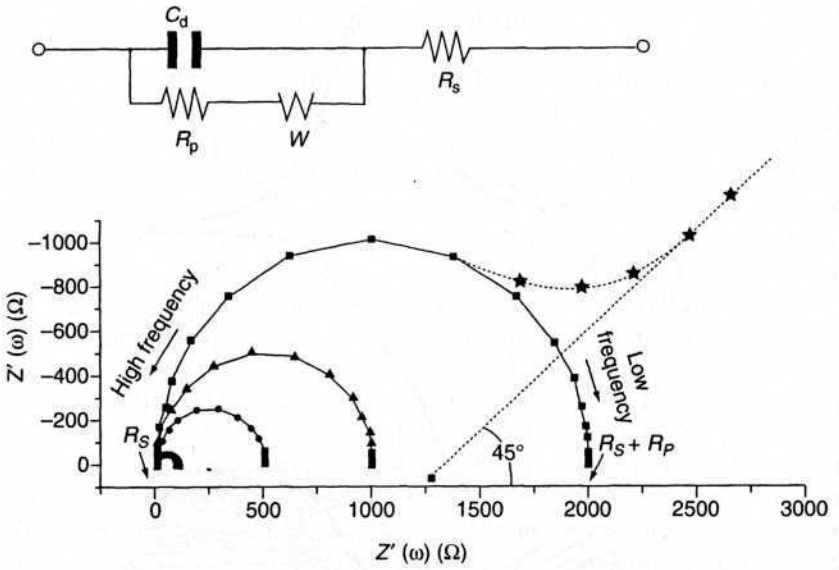

Figure 2.23 Faradaic impedance spectra presented in the form of Nyquist plots, along with the electronic equivalent circuit of the electrified interface. (Reproduced with permission from Ref. 87.)

$$Z(\omega) = R_s + R_p/(1+\omega^2 R_p^2 C_d^2) - j\omega R_p^2 C_d/(1+\omega^2 R_p^2 C_d^2) = Z' + jZ'' \qquad (2.20)$$

where $j = \sqrt{-1}$.

Impedance spectroscopy involves the application of a small-amplitude perturbing sinusoidal voltage signal (at a ω frequency) to the electrochemical cell and measuring the current response. The resulting faradaic impedance spectrum, known as a *Nyquist plot*, corresponds to the dependence of the imaginary number on the real number (e.g., Fig. 2.23), and contains extensive information about the electrified interface and the electron transfer reaction. Nyquist plots commonly include a semicircle region lying on the axis followed by a straight line. The semicircle portion (observed at higher frequencies) corresponds to the electron-transfer-limited process, while the straight line (characteristic of the low-frequency range) represents the diffusion-limited process. Such spectra can be used for extracting the electron transfer kinetics and diffusional characteristics. In the case of very fast electron transfer processes the impedance spectrum includes only the linear part, while very slow electron transfer processes are characterized by a large semicircular region. The diameter of the semicircle equals the electron transfer resistance. The intercepts of the semicircle with the Z_{re} axis correspond to those of R_s. In addition to fundamental electrochemical studies, the technique has been found extremely useful for transduction of bioaffinity events in connection to modern electrical immunosensors and DNA biosensors (88). Such transduction of bioaffinity events relies on the increased insulation of the electrode surface in respect to redox probes (e.g., ferrocyanide), present in the solution, on binding of large biomolecules (e.g., capture of an antigen that retards the electron transfer).

EXAMPLES

Example 2.1 The reversible oxidation of dopamine (DA) is a $2e^-$ process. A cyclic voltammetric anodic peak current of 2.2 μA is observed for a 0.4-mM solution of dopamine in phosphate buffer at a glassy carbon disk electrode of 2.6 mm^2 with a scan rate of 25 mV/s. What will i_p be for v = 100 mV/s and 1.2 mM DA?

Solution From Equation (2.1):

$$i_p = kCv^{1/2}$$
$$2.2 = k0.4(25)^{1/2}$$
$$k = 1.1$$

Under the new experimental conditions, i_p is given by

$$i_p = 1.1 \times 1.2 \times (100)^{1/2} = 13.2\,\mu A$$

Example 2.2 The following cyclic voltammogram was recorded for a reversible couple:

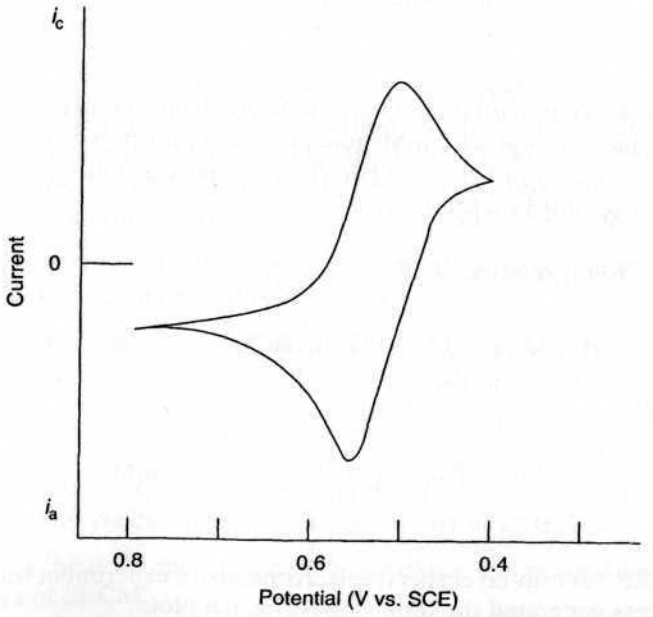

Calculate the number of electrons transferred and the formal potential for the couple.

Solution From Eq. (2.3):

$$n = 0.059/\Delta E_p = 0.059/(0.555 - 0.495) = 0.983 \cong 1.0$$

The formal potential can be calculated from Eq. (2.2):

$$E^\circ = (0.555 + 0.495)/2 = 0.525\,\text{V}$$

Example 2.3 The electropolymeric growth of 2 ng polyphenol onto a gold QCM crystal (A = 1 cm^2; f_0 = 5 MHz) resulted in a frequency change of 12.5 Hz. Calculate the frequency change associated with the deposition of 4 ng polyphenol onto a 0.5-cm^2 crystal (f_0 = 8 MHz).

Solution From Eq. (2.19):

$$\Delta f = -K\Delta m f_0^2/A$$
$$12.5 = -K\,2 \times 5^2/1 \qquad K = -0.25$$

Under the new experimental conditions, Δf is given by

$$\Delta f \cong -0.25 \times 4 \times 8^2/0.5 = 128\,\text{Hz}$$

Example 2.4 A potential-step spectroelectrochemistry experiment using a reactant concentration of 2 mM generated a product with an absorbance (sampled after 25 s) of 0.8. Calculate the reactant concentration that yielded an absorbance of 0.4 on sampling at 16 s.

Solution From Equation (2.17):

$$A = KC_O t^{1/2} \qquad 0.8 = K\,2(25)^{1/2} \qquad K = 0.08$$

Accordingly

$$0.4 = 0.08C_O(16)^{1/2} \qquad C_O = 5\,\text{mM}$$

Example 2.5 A thin-layer spectroelecrochemistry experiment for the O + ne$^-$ → R process generated the following Nernstian plot:

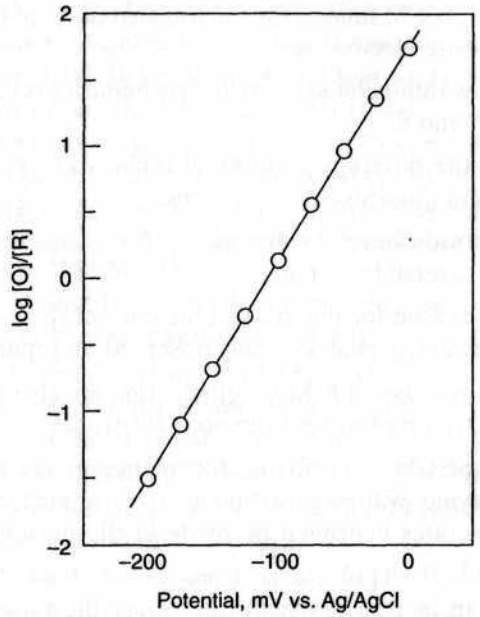

Calculate the number of electrons and formal potential of this redox process.

Solution The slope of this plot, 0.019 = 0.059/n, where n = 3. The intercept, 0.11 V, corresponds to the formal potential.

PROBLEMS

2.1 Explain and demonstrate how spectroelectrochemistry can provide useful information about a reaction mechanism involving a redox process followed by a chemical reaction (EC mechanism), involving decomposition of the reaction product. Draw absorbance–time signals for different rate constants of the decomposition reaction.

2.2 Which voltammetric technique can be used to estimate the surface coverage of an adsorbed molecule? How?

2.3 Draw an EQCM (mass–potential) profile for a metal deposition–stripping process during a cycling voltammetric scanning.

2.4 A cyclic voltammetric peak current of 12.5 μA was observed for the reversible reduction of a 1.5-mM lead solution using a 1.2-mm-diameter disk electrode and a 50 mV/s scan rate. Calculate the lead concentration that yields a peak current of 20.2 μA at 250 mV/s.

2.5 Discuss the difference between the feedback and generation/collection modes of SECM.

2.6 Explain how SECM images the microdistribution of the electrode activity of composite electrodes.

2.7 Describe how thin-layer spectroelectrochemistry is used to measure the values of E° and n.

2.8 Summarize the different features of cyclic voltammetric response for reversible and quasireversible systems.

2.9 Explain the use of cyclic voltammetry for estimating the values of E° and n for a reversible system.

2.10 What is the reason for the gradual increase of the cathodic and anodic cyclic voltammetric peak currents observed on repetitive scanning?

2.11 How would you use EQCM for elucidating the electrostatic desorption of anionic DNA molecules from gold electrodes?

2.12 Propose a SECM experiment for mapping the distribution of an oxidase enzyme within a carbon composite surface. (Note that the enzyme generates hydrogen peroxide in the presence of its substrate and oxygen.)

2.13 How does an increase in scan rate affect the ratio of peak currents (backward/forward) in a cyclic voltammetric experiment involving a redox process followed by a chemical reaction?

REFERENCES

1. Nicholson, R. S.; Shain, I., *Anal. Chem.* **36**, 706 (1964).
2. Echegoyen, L.; Echegoyen, L. E., *Acc. Chem. Res.* **31**, 593 (1998).
3. Andrieux, C. P.; Hapiot, P.; Savéant, J. M., *Electroanalysis* **2**, 183 (1990).
4. Gelbert, M. B.; Curran, D. J., *Anal. Chem.* **58**, 1028 (1986).
5. Hawley, M. D.; Tatawawdi, S. V.; Piekarski, S.; Adams, R. N., *J. Am. Chem. Soc.* **89**, 447 (1967).
6. Mohilner, D. M.; Adams, R. N.; Argersinger, W. R., *J. Am. Chem. Soc.* **84**, 3816 (1962).
7. Evans, D., *Acc. Chem. Res.* **10**, 313 (1977).
8. Mabbott, G., *J. Chem. Educ.* **60**, 697 (1983).
9. Rudolph, M.; Reddy, D.; Feldberg, S. W., *Anal. Chem.* **66**, 589A (1994).
10. Wang, J.; Luo, D. B.; Farias, P. A. M.; Mahmoud, J. S., *Anal. Chem.* **57**, 158 (1985).
11. Pearce, P. J.; Bard, A. J., *J. Electroanal. Chem.* **114**, 89 (1980).
12. Wopschall, R. H.; Shain, I., *Anal. Chem.* **39**, 1514 (1967).
13. Sluyters-Rehbach, M.; Sluyter, J. R., *J. Electroanal. Chem.* **65**, 831 (1975).
14. Brown, A. P.; Anson, F. C., *Anal. Chem.* **49**, 1589 (1977).
15. Stamford, J.; Hurst, P.; Kuhr, W.; Wightman, R. M., *J. Electroanal. Chem.* **265**, 291 (1989).
16. Baur, J.; Kristensen, E.; May, L.; Wiedemann, D.; Wightman, R. M., *Anal. Chem.* **60**, 1268 (1988).

17. Venton, B.; Wightman, R. M., *Anal. Chem.* **75**, 414A (2003).
18. Michael, D.; Travis, E.; Wightman, R. M., *Anal. Chem.* **70**, 586A (1998).
19. Jackson, B.; Dietz, S.; Wightman, R. M., *Anal. Chem.* **67**, 1115 (1995).
20. Heinze, J., *Angew Chem. (Int. Ed. Engl.)* **23**, 831 (1984).
21. Baldwin, R. P.; Ravichandran, K.; Johnson, R. K., *J. Chem. Ed.* **61**, 820 (1984).
22. Kuwana, T.; Heineman, W., *Acc. Chem. Res.* **9**, 241 (1976).
23. Heineman, W.; Hawkridge, F.; Blount, H., "Spectroelectrochemistry at optically transparent electrodes," in A. J. Bard, ed., *Electroanalytical Chemistry*, Marcel Dekker, New York, 1986, Vol. 13.
24. Van Dyke, D. A.; Cheng, H. Y., *Anal. Chem.* **60**, 1256 (1988).
25. Porter, M.; Kuwana, T., *Anal. Chem.* **56**, 529 (1984).
26. Brewster, J.; Anderson, J. L., *Anal. Chem.* **54**, 2560 (1982).
27. Norvell, V.; Mamantov, G., *Anal. Chem.* **49**, 1470 (1977).
28. Heineman, W. R., *J. Chem. Educ.* **60**, 305 (1983).
29. Bancroft, E.; Sidwell, J.; Blount, H., *Anal. Chem.* **53**, 1390 (1981).
30. Gui, Y. P.; Porter, M.; Kuwana, T., *Anal. Chem.* **57**, 1474 (1985).
31. Shi, Y.; Slaterbeck, A.; Seliskar, C.; Heineman, W. R., *Anal. Chem.* **69**, 3676 (1997).
32. Dewald, H. D.; Wang, J., *Anal. Chim. Acta* **166**, 163 (1984).
33. Faulkner, L.; Bard, A. J., "Electrochemiluminescence," in A. J. Bard, ed., *Electroanalytical Chemistry*, Marcel Dekker, New York, 1977, Vol. 10.
34. Velasco, J. G., *Electroanalysis* **3**, 261 (1991).
35. White, H. S.; Bard, A. J., *J. Am. Chem. Soc.* **104**, 6891 (1982).
36. Richter, M. M., *Chem. Rev.* **104**, 3003 (2004).
37. Knight, A. W.; Greenway, G., *Analyst* **119**, 879 (1994).
38. Kulmala, S.; Suomi, J., *Anal. Chim. Acta* **500**, 21 (2003).
39. Forry, S. P.; Wightman, R. M., *Anal. Chem.* **74**, 528 (2002).
40. Zhan, W.; Alvarez, J.; Crooks, R. M., *J. Am. Chem. Soc.* **124**, 13265 (2002).
41. Bagchi, R. N.; Bond, A. M.; Scholz, F., *Electroanalysis* **1**, 1 (1989).
42. Richards, J. A.; Evans, D. H., *Anal. Chem.* **47**, 964 (1965).
43. Chang, H.; Johnson, D. C.; Houk, R. S., *Trends Anal. Chem.* **8**, 328 (1989).
44. Regino, M. C.; Brajter-Toth, A., *Anal. Chem.* **69**, 5067 (1997).
45. Tong, Y.; Oldfield, E.; Wieckowski, A., *Anal. Chem.* **70**, 518A (1998).
46. Jeanmarie, D.; Van Duyne, R., *J. Electroanal. Chem.* **84**, 1 (1977).
47. McCreery, R. L.; Packard, R. T., *Anal. Chem.* **61**, 775A (1989).
48. Abruna, H. D., *Electrochemical Interfaces*, VCH Publishers, New York, 1991.
49. Arvia, A. J., *Surf. Sci.* **181**, 78 (1987).
50. Cataldi, T. R.; Blackham, I.; Briggs, A.; Pethica, J.; Hill, H. A., *J. Electroanal. Chem.* **290**, 1 (1990).
51. Wang, J., *Analyst* **117**, 1231 (1992).
52. Wang, J.; Martinez, T.; Yaniv, D.; McCormick, L. D., *J. Electroanal. Chem.* **278**, 379 (1990).
53. Widrig, C.; Alves, C.; Porter, M., *J. Am. Chem. Soc.* **113**, 2805 (1991).
54. Kim, T.; Yang, H.; Bard, A., *J. Electrochem. Soc.* **138**, L71 (1991).
55. Wang, J.; Martinez, T.; Yaniv, D.; McCormick, L. D., *J. Electroanal. Chem.* **286**, 265 (1990).

56. Hansma, H.; Weisenhorm, A.; Edmundson, A.; Gaub, H.; Hansma, P., *Clin. Chem.* **37**, 1497 (1991).
57. Gardner, C. E.; Macpherson, J. V., *Anal. Chem.* **74**, 576A (2002).
58. Jones, V.; Kenseth, J.; Porter, M. D.; Mosher, C. L.; Henderson, E., *Anal. Chem.* **70**, 1233 (1998).
59. Demers, L. M.; Ginger, D.; Park, S.; Li, Z.; Chung, S.; Mirkin, C. A., *Science* **296**, 1836 (2002).
60. Liu, W.; Montana, V.; Chapman, E. R.; Mohideen, U.; Parpura, V., *Proc. Natl. Acad. Sci. USA* **100**, 13621 (2003).
61. Wickramaasinghe, H., *Scientific Am.* **98** (Oct. 1989).
62. Engstrom, R.; Pharr, C., *Anal. Chem.* **61**, 1099A (1989).
63. Bard, A. J.; Denuault, G.; Lee, C.; Mandler, D.; Wipf, D., *Acc. Chem. Res.* **23**, 357 (1990).
64. Mirkin, M. V., *Anal. Chem.* **68**, 177A (1996).
65. Arca, M.; Bard, A. J.; Horrocks, B.; Richards, T.; Treichel, D., *Analyst* **119**, 719 (1994).
66. Liu, H.; Fan, F.; Lin, C.; Bard, A. J., *J. Am. Chem. Soc.* **108**, 3838 (1986).
67. Kwak, J.; Bard, A. J., *Anal. Chem.* **61**, 1794 (1989).
68. Fan, F.; Kwak, J.; Bard, A. J., *J. Am. Chem. Soc.* **118**, 9669 (1996).
69. Wang, J.; Wu, L.; Li, R., *J. Electroanal. Chem.* **272**, 285 (1989).
70. Pierce, D.; Unwin, P.; Bard, A. J., *Anal. Chem.* **64**, 1795 (1992).
71. Bath, B. D.; Scott, E. R.; Phipps, J. B.; White, J. S., *J. Pharm. Sci.* **89**, 1537 (2000).
72. Yasukawa, T.; Kaya, T.; Matsue, T., *Electroanalysis* **12**, 653 (2000).
73. Yamashita, K.; Takagi, M.; Uchida, K.; Kondo, H.; Takenak, S., *Analyst* **126**, 1210 (2001).
74. Horrocks, B.; Mirkin, M.; Pierce, D.; Bard, A. J.; Nagy, G.; Toth, K., *Anal. Chem.* **65**, 1304 (1993).
75. Wei, C.; Bard, A. J.; Nagy, G.; Toth, K., *Anal. Chem.* **67**, 1346 (1995).
76. Nowall, W.; Wipf, D.; Kuhr, W. G., *Anal. Chem.* **70**, 2601 (1998).
77. *Scanning Electrochemical Microscope*, CH Instruments, 1998.
78. Smith, J. P., *Anal. Chem.* **73**, 39A (2001).
79. Kranze, C.; Friedbacher, G.; Mizaikoff, B.; Lugstein, A.; Smoliner, J.; Bertagnolli, E., *Anal. Chem.* **73**, 2491 (2001).
80. Boldt, F.; Heinze, J.; Diez, M.; Peterson, J.; Börsch, M., *Anal. Chem.* **76**, 3473 (2004).
81. Basak, S.; Bose, C.; Rajeshwar, K., *Anal. Chem.* **64**, 1813 (1992).
82. Hillman, A. R.; Loveday, D.; Swann, M.; Bruckenstein, S.; Wildle, C. P., *Analyst* **117**, 1251 (1992).
83. Deakin, M.; Buttry, D., *Anal. Chem.* **61**, 1147A (1989).
84. Ward, M. D.; Buttry, D. A., *Science* **249**, 1000 (1990).
85. Cliffel, D.; Bard, A. J., *Anal. Chem.* **70**, 1993 (1998).
86. Tatsuma, T.; Watanabe, Y.; Oyama, N.; Kiakizaki, K.; Haba, M., *Anal. Chem.* **71**, 3632 (1999).
87. Park, S. M.; Yoo, J. S., *Anal. Chem.* **75**, 455A (2003).
88. Katz, E.; Willner, I., *Electroanalysis* **15**, 913 (2003).

3

CONTROLLED-POTENTIAL TECHNIQUES

The basis of all controlled-potential techniques is the measurement of the current response to an applied potential. A multitude of potential excitations (including a ramp, potential steps, pulse trains, a sine wave, and various combinations thereof) exists. The present chapter reviews those techniques that are widely used.

3.1 CHRONOAMPEROMETRY

Chronoamperometry involves stepping the potential of the working electrode from a value at which no faradaic reaction occurs to a potential at which the surface concentration of the electroactive species is effectively zero (Fig. 3.1a). A stationary working electrode and unstirred (quiescent) solution are used. The resulting current–time dependence is monitored. As mass transport under these conditions is solely by diffusion, the current–time curve reflects the change in the concentration gradient in the vicinity of the surface (recall Section 1.2). This involves a gradual expansion of the diffusion layer associated with the depletion of the reactant, and hence decreased slope of the concentration profile as time progresses (see Fig. 3.1b). Accordingly, the current (at a planar electrode) decays with time (Fig. 3.1c), as given by the *Cottrell equation*

Analytical Electrochemistry, Third Edition, by Joseph Wang